NASA Technical Memorandum 105893

# Supersonic Boundary-Layer Flow
# Turbulence Modeling

Chi-Rong Wang
*Lewis Research Center*
*Cleveland, Ohio*

NASA

Supersonic Boundary-Layer Flow Turbulence Modeling

Chi-Rong Wang

Heat Transfer Branch, Internal Fluid Mechanics Division,
NASA Lewis Research Center, Cleveland, Ohio 44135, U.S.A.

**Abstract**
Baldwin-Lomax and k-ε turbulence models were modified for use in Navier-Stokes numerical computations of Mach 2.9 supersonic turbulent-boundary-layer flows along compression ramps. The computational results of Reynolds shear stress profiles were compared with experimental data. The Baldwin-Lomax model was modified to account for the Reynolds shear stress amplification within the flow field. A hybrid k-ε model with viscous sublayer turbulence treatment was constructed to predict the Reynolds shear stress profiles within the entire flow field. These modified turbulence models were effective for the computations of the surface pressure and the skin friction factor variations along an 8° ramp surface. The hybrid k-ε model could improve the predictions of the Reynolds shear stress profile and the skin friction factor near the corner of a 16° ramp.

## 1. INTRODUCTION

Shock-wave/turbulent-boundary-layer interaction is an important phenomenon which occurs in high-speed flow fields. Delery, Marvin, and Reshotko (ref. 1) have reviewed the literature on shock-wave/boundary-layer interaction in transonic and supersonic speeds. In their review, they describe flow phenomena based on experimental observations and theoretical concepts. Numerical solutions of the compressible Navier-Stokes equations and energy equation have been used by many researchers to predict the surface pressure and skin friction of flow fields with shock-wave/turbulent-boundary-layer interaction. The Reynolds analogy is usually used to relate the turbulent thermal flux to the turbulent momentum flux. Thus, accurate modeling of the turbulent shear stress is essential to the success of the Navier-Stokes computations.

This paper describes some of the turbulence modeling techniques used in the Navier-Stokes computations of two-dimensional supersonic flow with shock-wave/turbulent-boundary-layer interaction. Flow fields around 8° and 16° compression ramps imbedded in fully developed turbulent-boundary-layer flows were considered in this study. (See fig. 1.) The free-stream Mach number for the flow fields considered was 2.9. A time-dependent explicit Navier-Stokes computational code (ref. 2) was used for the present computations. The Baldwin-Lomax turbulence model (ref. 3) was used first to model the turbulent eddy viscosity. This turbulence model was modified so that prediction of the Reynolds shear stress measurements could be made. A compressible k-ε turbulence model (ref. 4) was then used to model the turbulent eddy viscosity of the supersonic, flat-plate turbulent boundary layer. The high-Reynolds-number form of the k-ε turbulence model and a viscous sublayer turbulence model (ref. 5) were combined to formulate a hybrid turbulence model for the flow along a compression ramp. The computed Reynolds shear stress and mean flow properties within the compression ramp flows are described and compared with experimental measurements (ref. 6).

## 2. SYMBOLS

| | |
|---|---|
| $C_f$ | skin friction factor, $\tau_w/0.5\,\rho_\infty U_\infty$ |
| $C_i$, $C_o$, $C_{kleb}$, $C_\mu$, $C_v$ | empirical constants |
| Re | Reynolds number, $\rho_\infty U_\infty \delta/U_\infty$ |
| U, V | mass-averaged velocity components |
| $U_\tau$ | frictional velocity, $(\tau_w/\rho_w)^{0.5}$ |
| X, Y | physical coordinates |
| $Y^+$ | $\rho_w U_\tau Y/\mu_w$ |
| k | mass-averaged turbulent kinetic energy |
| p | surface pressure |
| $\delta$ | boundary layer thickness |
| $\delta_{ij}$ | Kronecker delta |
| $\epsilon$ | mass-averaged turbulent dissipation rate |
| $\mu_t$ | turbulent eddy viscosity |
| $\mu$ | dynamic viscosity |
| $\rho$ | mass-averaged density |
| $\tau_{xy}$ | Reynolds shear stress, $\mu_t(\partial U/\partial Y + \partial V/\partial X)$ |
| $\tau_w$ | surface shear stress, $\mu_w(\partial U/\partial Y)\big|_{Y=0}$ |
| $\omega$ | vorticity, $(\partial U/\partial Y) - (\partial V/\partial X)$ |

Subscripts:

| | |
|---|---|
| c | condition at ramp corner |
| s | sublayer condition |
| v | sublayer edge condition |
| w | wall surface condition |
| 0 | condition at X = 0 |
| $\infty$ | free-stream condition |

## 3. TURBULENCE MODELS

This section describes the Baldwin-Lomax and k-$\epsilon$ models, which have been widely used to model the turbulence in the computations of various types of turbulent flows.

### 3.1. Baldwin-Lomax Turbulence Model

The Baldwin-Lomax turbulence model is a two-layer eddy viscosity model (ref. 3). The eddy viscosity of a two-dimensional boundary layer can be written as follows:

In the inner layer, the eddy viscosity $\mu_{t,i}$ is given by

$$\mu_{t,i} = \rho\left[C_i Y\left(1 - e^{-Y^+/26}\right)\right]^2 |\omega| \tag{1}$$

In the outer layer, the eddy viscosity $\mu_{t,o}$ is given by

$$\mu_{t,o} = 0.0168 C_o \rho \, F_{wake} F_{kleb} \tag{2}$$

where

$F_{wake}$ is the minimum of

$$|Y_{max} F_{max}$$

$$|0.25 Y_{max} U^2_{dif} / F_{max}$$

and

$$F = Y|\omega| \left( 1 - e^{-Y^+/26} \right)$$

The quantity $F_{max}$ is the maximum value of $F$ and $Y_{max}$ is the value of $Y$ at which $F_{max}$ occurs. The function $F_{kleb}$ is the Klebanoff intermittency factor given by

$$F_{kleb} = 1 / \left[ 1 + 5.5(C_{kleb} Y / Y_{max})^6 \right] \tag{3}$$

The quantity $U_{dif}$ is the difference between the maximum and minimum velocities.

$$U_{dif} = \left( \sqrt{U^2 + V^2} \right)_{max} - \left( \sqrt{U^2 + V^2} \right)_{min}$$

The $\left( \sqrt{U^2 + V^2} \right)_{min}$ term in $U_{dif}$ was set to be zero in this study.

The empirical constants $C_i$, $C_o$, and $C_{kleb}$ appearing in equations (1) to (3) were previously determined (ref. 3) for constant-pressure boundary layers at transonic speeds. In this study, these empirical constants were adjusted to achieve better prediction of the Reynolds shear stress in the supersonic compression ramp flow field. Different sets of these empirical constants were found to model the turbulence eddy viscosity upstream and downstream of the compression corner. These new sets of empirical constants are (1) $C_i = 0.41$, $C_o = 1$ and $C_{kleb} = 0.8$ for the upstream modeling, $X < X_c$, and (2) $C_i = 0.45$, $C_o = 2$, and $C_{kleb} = 0.8$ for the downstream modeling, $X > X_c$.

### 3.2. Hybrid k-ε turbulence model

Nichols (ref. 4) extended an incompressible k-ε turbulence model (ref. 7) to include the effect of compressibility. Based on the existing turbulence modeling technique (ref. 4), the following compressible k-ε turbulence model was used to predict the turbulent eddy viscosity within the supersonic, flat-plate turbulent-boundary-layer flow.

The turbulent eddy viscosity was defined as

$$\mu_t = \rho C_\mu (k^2/\varepsilon) \left( 1 - e^{-0.0115 \rho U_r Y / \mu} \right) \tag{4}$$

with $C_\mu = 0.09$.

The turbulent kinetic energy and the dissipation rate were described by using the following transport equations:

$$\frac{\partial}{\partial t}(\rho k) + \frac{\partial}{\partial X}(\rho U k) + \frac{\partial}{\partial Y}(\rho V k) = \frac{\partial}{\partial X}\left[ (\mu + \mu_t)\frac{\partial k}{\partial X} \right] + \frac{\partial}{\partial Y}\left[ (\mu + \mu_t)\frac{\partial k}{\partial Y} \right]$$

$$+ P - \rho\varepsilon - \frac{2\mu k}{Y^2} \tag{5}$$

3

$$\frac{\partial}{\partial t}(\rho\varepsilon) + \frac{\partial}{\partial X}(\rho U\varepsilon) + \frac{\partial}{\partial Y}(\rho V\varepsilon) = \frac{\partial}{\partial X}\left[(\mu + \frac{\mu_t}{1.3})\frac{\partial\varepsilon}{\partial X}\right] + \frac{\partial}{\partial Y}\left[(\mu + \frac{\mu_t}{1.3})\frac{\partial\varepsilon}{\partial Y}\right]$$

$$+ 1.35\,\frac{\varepsilon}{k}\,P - \frac{\varepsilon}{k}\,(1.8 f \rho\varepsilon + \frac{\partial\mu k e^{-0.5\rho U_r Y/\mu}}{Y^2}) \tag{6}$$

where

$$f = 1 - \frac{0.2}{0.9}\,e^{-(k^2\rho/6\mu\varepsilon)^2} \tag{7}$$

Some additional terms (ref. 4) to account for the compressibility effect on the transport of the turbulent kinetic energy were not retained in equation (5). The production term P was defined as

$$P = \left\{\mu_t\left[\left(\frac{\partial U_i}{\partial X_j} + \frac{\partial U_j}{\partial X_i}\right) - \frac{2}{3}\frac{\partial U k}{\partial X_k}\delta_{ij}\right] - \frac{2}{3}\rho k\delta_{ij}\right\}\frac{\partial U_i}{\partial X_j}$$

Equations (4) to (7) were also solved for the turbulent eddy viscosity in the computations of the flow along the compression ramp. The source terms were found to be numerically stiff at locations near the compression corner. Therefore, a viscous sublayer model (ref. 5) was used to eliminate the stiffness problem. This viscous sublayer model and the high-Reynolds-number forms of the k-$\varepsilon$ turbulence model corresponding to equations (4) to (6) were combined to formulate a hybrid k-$\varepsilon$ turbulence model for the flow over the compression ramp.

To implement the sublayer model, it was assumed that

(1) Adjacent to the wall, the viscous sublayer thickness $Y_v$ is defined by

$$Y_v = 20\,(\mu_w/\rho_w)\,C_v^{0.25}/U_r \tag{8}$$

where $C_v$ is an empirical constant discussed later. The turbulent kinetic energy, the dissipation rate, and the eddy viscosity at the sublayer edge are given by

$$k_v = (U_r^2/C_v^{0.5})\,(\rho_w/\rho_v) \tag{9}$$

$$\varepsilon_v = (U_r^3/0.4 Y_v)\,(\rho_w/\rho_v)^{1.5} \tag{10}$$

and

$$\mu_{t,v} = C_\mu \rho_v k_v^2/\varepsilon_v \tag{11}$$

(2) Within the viscous sublayer, $0 < Y < Y_v$, the turbulent kinetic energy and the dissipation rate are given by

$$k_s = (\rho_v/\rho_s)k_v(Y_s/Y_v)^2 \tag{12}$$

and

$$\varepsilon_s = 2(\mu_w/\rho_w)\left(k_v/Y_v^2\right) \tag{13}$$

By substituting equations (9) and (10) into equation (11), the following eddy viscosity expression is established:

4

$$\mu_{t,v} = 0.4(C_\mu/C_v)\mu_w Y_v^+ (\rho_v/\rho_w)^{0.5} \tag{14}$$

It was further assumed that equation (11) holds near the sublayer edge. By substituting equations (12) and (13) in equation (11) and taking the limit as $Y$ approaches $Y_v$, the following eddy viscosity expression is found:

$$\mu_{t,v} = 0.5\left(C_\mu/C_v^{0.5}\right)\mu_w Y_v^{+^2} \tag{15}$$

Therefore, the eddy viscosity satisfying equations (14) and (15) and the limiting condition at $Y_v$ has the following form:

$$\mu_{t,s} = C_s(Y)\,(\rho/Y^+)\left(k_s^2/\varepsilon_s\right) \tag{16}$$

$C_s(Y)$ is assumed to be linear in the direction normal to the surface, that is,

$$C_s(Y) = C_\mu + \left(C_{sv} - C_\mu\right)Y/Y_v \tag{17}$$

By substituting $C_s(Y)$ into equation (16) and evaluating the eddy viscosity at the sublayer edge, the expression

$$C_{sv} = 0.8\left(C_\mu/C_v^{0.5}\right)(\rho_v/\rho_w)^{0.5} \tag{18}$$

can be obtained. Thus, the expression for the eddy viscosity within the viscous sublayer becomes

$$\mu_{t,s} = \left\{C_\mu + [0.8(C_\mu/C_v^{0.5})\,(\rho_v/\rho_w)^{0.5} - C_\mu]\,Y/Y_v\right\}(\rho/Y^+)k_s^2/\varepsilon_s \tag{19}$$

The viscous sublayer thickness is an important parameter of this sublayer turbulence model. For a fully developed flat-plate turbulent-boundary-layer flow with Mach 3 free stream, experiments (ref. 8) have established the correlation

$$Y_v/\delta = 7.92\times10^2 Re^{-0.91} \tag{20}$$

among the boundary layer thickness, the Reynolds number, and the viscous sublayer thickness. Based on the present flat-plate turbulent-boundary-layer conditions (Fig. 1), this correlation gave a viscous sublayer thickness of $4.8\times10^{-2}$ mm. With the same boundary-layer flow conditions, equation (8) predicted the sublayer thickness when $C_v$ has a value of approximately 0.4. Therefore, a $C_v$ of 0.4 was assumed for the viscous-sublayer eddy viscosity expression given by equation (19).

In this study, equations (12), (13), and (19) were used to calculate the turbulent kinetic energy, the dissipation rate, and the eddy viscosity within the attached viscous sublayer. The high-Reynolds-number forms of equations (4) to (6) were solved numerically for similar turbulence quantities at locations outside the viscous sublayer.

## 4. COMPUTATIONAL METHOD

For this study, a time-dependent explicit numerical code (ref. 2) was used. Initially, this code used only the Baldwin-Lomax eddy viscosity model. The code was modified by adding the hybrid k-$\varepsilon$ turbulence model to the numerical procedures. The conservation equations, the

coordinate transformations between the physical and the computational domains, and the finite difference scheme used are described in reference 9. A computational domain of $7\delta$ in the X-direction and $2\delta$ in the Y-direction was used for the 8° compression ramp computation, and a domain of $7.5\delta$ in the X-direction and $2.5\delta$ in the Y-direction were used for the 16° compression ramp computation. These domains were chosen so that the shock waves crossed the downstream outflow boundary. Typically, a 221×149 mesh size was used for the present computations. The grid configuration was packed near the surface and around the compression corner. There were 12 grid points within the viscous sublayer.

First, the turbulent flat-plate boundary-layer flow properties were calculated. The 1/7th-power-law velocity profile was used as the initial mean flow velocity. The initial temperature profile was determined from the velocity and temperature relation of a compressible laminar boundary layer along a heated plate (ref. 10). Nonslip boundary conditions and constant wall temperature were used for the surface boundary conditions. The incompressible flat-plate boundary-layer turbulent kinetic energy profile (ref. 11) was used as the initial condition. The corresponding dissipation rate was calculated by using $\varepsilon = \rho C_\mu k^2 / \mu_t$, where $\mu_t$ was obtained from the Baldwin-Lomax model. The flat-plate boundary-layer flow properties were then used as the initial conditions to start the compression ramp flow computations. The free-stream properties (ref. 6) were used as the far-field boundary conditions.


## 5. RESULTS AND DISCUSSION

In this section, the computational results for the flow properties, especially the Reynolds stresses, are described and compared with measurements of reference 6.

### 5.1. Flat-plate turbulent-boundary-layer flow

The computed Reynolds shear stress profiles with the standard and revised Baldwin-Lomax turbulence models and the low-Reynolds-number k-$\varepsilon$ two-equation model are plotted in Figure 2. The standard Baldwin-Lomax model calculated larger Reynolds shear stress at locations away from the wall surface. By changing the value of $C_{kleb}$ from 0.3 to 0.8, and thus changing the Klebanoff intermittency factor (eq. (3)), the Baldwin-Lomax model can predict the experimentally measured Reynolds shear stress levels. The low-Reynolds-number k-$\varepsilon$ turbulence model (eqs. (4) to (7)) predicted the Reynolds shear stress measurements within the entire boundary layer. Particularly noteworthy, this turbulence modeling technique could describe the near-wall Reynolds shear stress variation as shown by the experimental results. The present computations also predicted a skin friction factor $C_{f,0}$ of 0.00095, which agrees with the measurement (ref. 6).

### 5.2. Eight-degree compression ramp flow

The computed Reynolds shear stress distributions along the Y-direction at five different $X/\delta$ locations of the 8° compression ramp are shown in Figure 3. The Baldwin-Lomax model predicted lower downstream shear stress than the measured values. The modified Baldwin-Lomax model calculated larger downstream Reynolds shear stress levels, which agrees with the measurement. The present computations predicted the Reynolds shear stress variation within the entire flow field when the hybrid k-$\varepsilon$ model with $C_\mu = 0.075$ was used for turbulence modeling. Preliminary study indicated that the requirement of this $C\mu$ value was due to the grid configuration used in the computation.

The computed skin friction factor and surface pressure variations along the surface of the compression ramp are shown in Figure 4. The experimental surface pressure distribution can be predicted by using either the original or the modified Baldwin-Lomax model. The

6

computations indicate a higher level of the skin friction downstream of the compression corner when the modified Baldwin-Lomax model was used for turbulence modeling. This skin friction distribution agrees better with the measurements. The computation using the hybrid k-ε turbulence model also predicted approximately the experimental surface pressure and skin friction distributions.

### 5.3. Sixteen-degree compression ramp flow

The computed Reynolds shear stress variations in the Y-direction at five different $X/\delta$ locations downstream of the corner are shown in figure 5. Both the modified Baldwin-Lomax model and the hybrid k-ε model could predict the Reynolds shear stress profile only at the far downstream location $(X/\delta = 6.5)$. However, the hybrid k-ε turbulence model prediction seems to show an improved prediction of the Reynolds stress profiles near the compression corner.

The computed skin friction factor and surface pressure variations along the 16° compression ramp surface are compared with the experimental measurements in Figure 6. The computations, using the Baldwin-Lomax model, closely predicted the surface pressure measurements. However, the computational results of the skin friction factor are in poor agreement with the experimental data. When the hybrid k-ε model with $C_\mu = 0.09$ was used for turbulence modeling, the computation accurately predicted the downstream skin friction variation, and a lower level of the downstream surface pressure was computed. A large compression angle (16°) might cause the viscous sublayer thickness to be reduced downstream of the compression corner. In order to model this behavior, a smaller sublayer thickness (80 percent of its upstream value) at the locations downstream of the compression corner was used in this part of the computations. Without the reduction in the sublayer thickness, the computations would predict a lower level of the downstream skin friction.

## 6. CONCLUSIONS

An application of turbulence modeling techniques used in the Navier-Stokes computations of two-dimensional, turbulent-boundary-layer flow with shock wave interaction was investigated. The supersonic flow fields due to 8° and 16° compression ramps imbedded in fully developed turbulent-boundary-layer flows were considered in this study. The free-stream Mach number of the flows considered was 2.9. Based on the results of this study, the following conclusions can be made:

1. The Klebanoff intermittency factor of the Baldwin-Lomax turbulence model must be modified for the model to predict the Reynolds shear stress profile within the flat-plate supersonic turbulent boundary layer. Some empirical constants of this turbulence model were also adjusted for the model to estimate the downstream Reynolds shear stress of a compression ramp flow.

2. A hybrid k-ε turbulence model, using viscous sublayer model for near-wall turbulence treatment, was constructed for the computation of supersonic boundary layer flow along compression ramps. The viscous sublayer thickness was an important parameter of the model. An experimental correlation for the sublayer thickness was used to resolve the effect of the sublayer thickness on the turbulence model.

3. When the modified Baldwin-Lomax model or the hybrid k-ε model was used in the computations of the flow over an 8° compression ramp, the computation could predict the experimental results of the Reynolds shear stress profiles within the entire flow field. The computational results of the surface pressure and the skin friction factor were found to agree well with their measured values.

4. The computations could predict only the Reynolds shear stress profile at far downstream locations when the modified Baldwin-Lomax model or the hybrid k-ε model was used in the computations of the flow over 16° compression ramp. However, the hybrid k-ε model improved the predictions of the Reynolds shear stress profiles and the surface skin friction factors immediately downstream of the compression corner.

## 7. REFERENCES

1. J. Delery, J.G. Marvin, and E. Reshotko, AGARD AG-280 (1986).
2. J.S. Shang, W.L. Hankey, and C.H. Law, AIAA J., 14, (1976) 1451.
3. B. Baldwin and H. Lomax, AIAA Paper 78-257 (1978).
4. R.H. Nichols, AIAA Paper 90-0494 (1990).
5. J.J. Gorski, AIAA Paper 86-0556 (1986).
6. A.J. Smits and K.C. Muck, J. Fluid Mech., 182 (1987) 291.
7. K.Y. Chien, AIAA J., 20, (1982) 33.
8. G.S. Settles, Ph. D. Dissertation, Aerospace and Mechanical Sciences Department, Princeton University (1975).
9. C.R. Wang, W.R. Hingst, and A.R. Porro, NASA CP-3078 (1991) 429.
10. H. Schlichting, Boundary-Layer Theory, McGraw-Hill, (1968) 317.
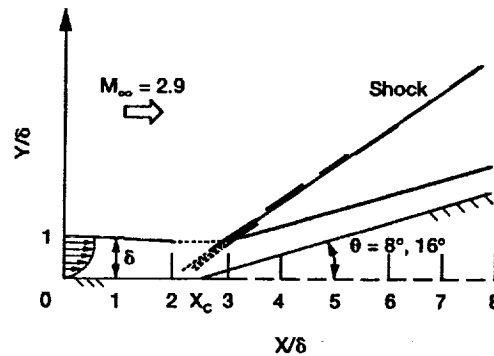11. P.S. Klebanoff, NACA TN-3178, (1955).

Figure 1.—Compression ramp flow model ($\delta$ = 26 mm, Re = $\rho_\infty U_\infty \delta / \mu_\infty$ = 1.76x10$^6$).
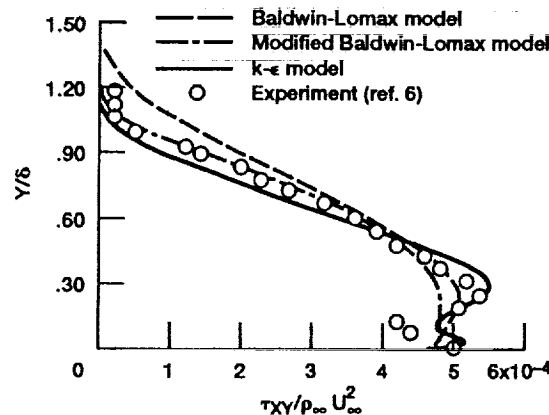


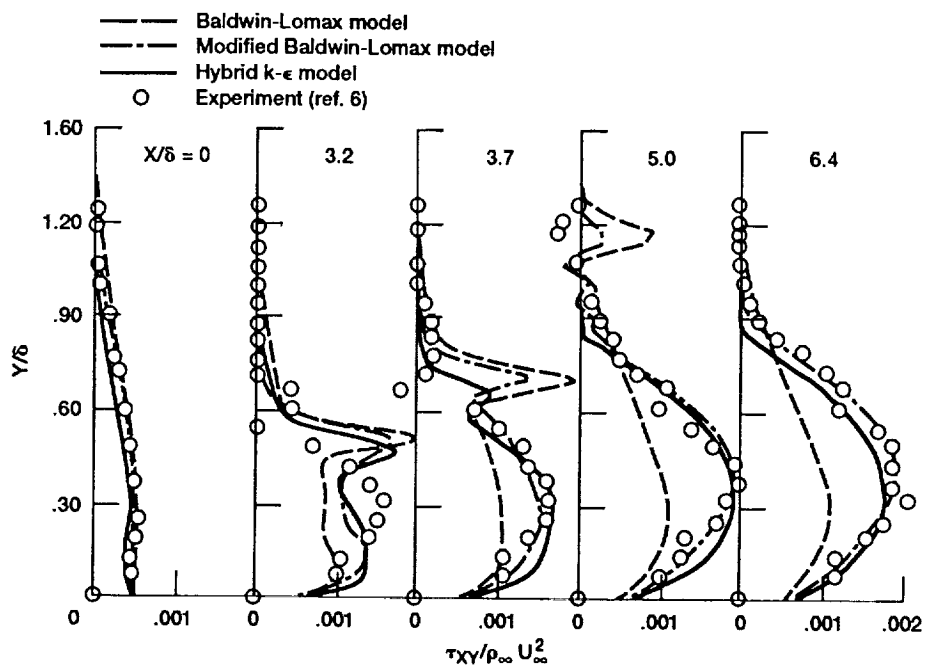Figure 2.—Boundary-layer-flow Reynolds shear stress profiles.

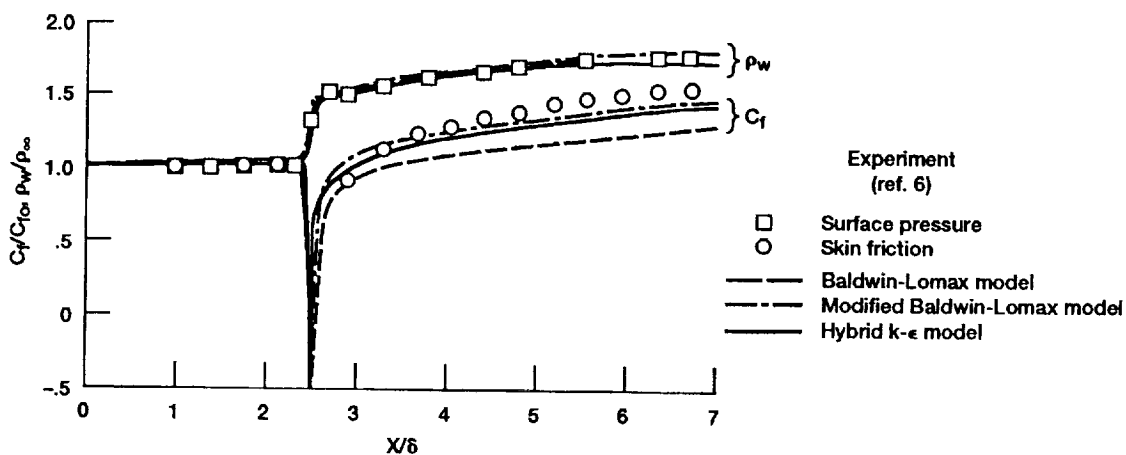Figure 3.—Reynolds shear stress profiles of 8° compression ramp.



Figure 4.—Surface pressure and skin friction factor of 8° compression ramp.
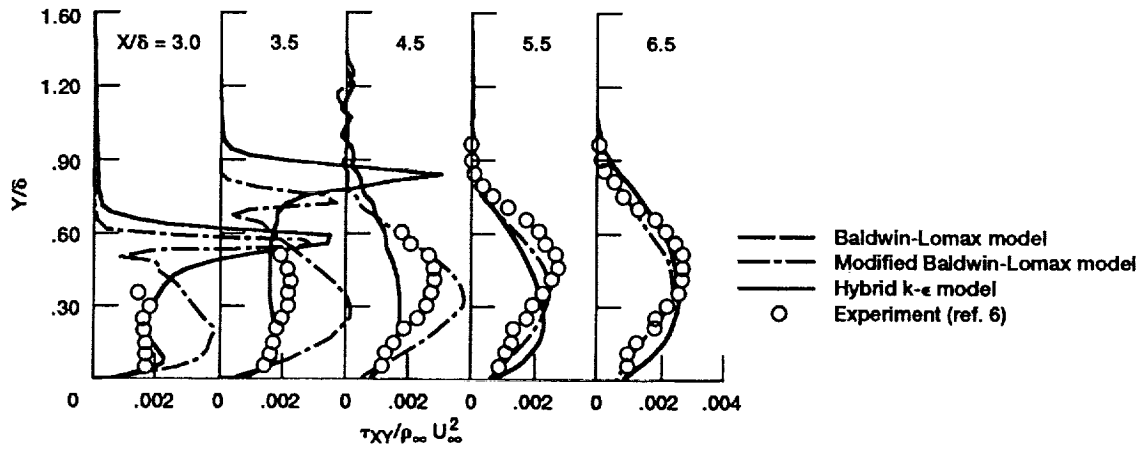
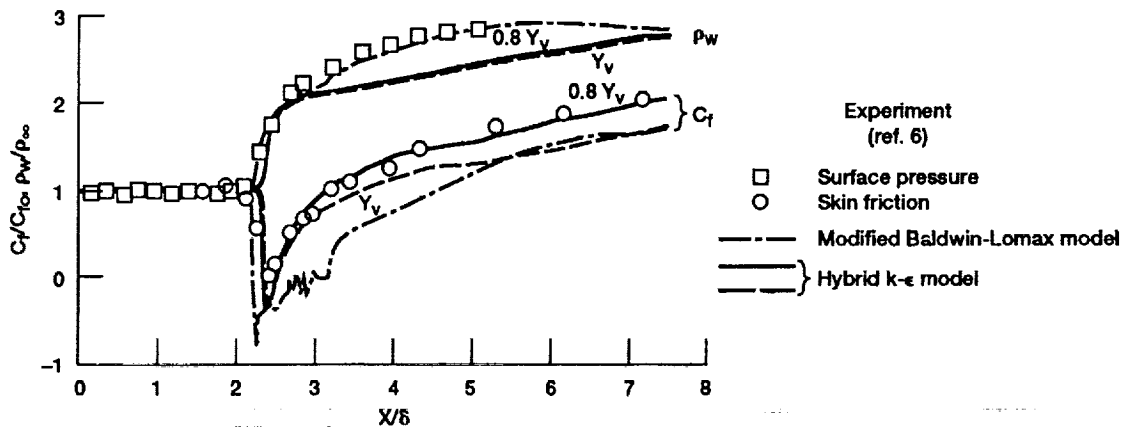Figure 5.—Reynolds shear stress profiles of 16° compression ramp.



Figure 6.—Surface pressure and skin friction factor of 16° compression ramp.

10

# REPORT DOCUMENTATION PAGE

Public reporting burden for this collection of information is estimated to average 1 hour per response, including the time for reviewing instructions, searching existing data sources, gathering and maintaining the data needed, and completing and reviewing the collection of information. Send comments regarding this burden estimate or any other aspect of this collection of information, including suggestions for reducing this burden, to Washington Headquarters Services, Directorate for information Operations and Reports, 1215 Jefferson Davis Highway, Suite 1204, Arlington, VA 22202-4302, and to the Office of Management and Budget, Paperwork Reduction Project (0704-0188), Washington, DC 20503.

| 1. AGENCY USE ONLY (Leave blank) | 2. REPORT DATE<br>March 1993 | 3. REPORT TYPE AND DATES COVERED<br>Technical Memorandum |
|---|---|---|

**4. TITLE AND SUBTITLE**

Supersonic Boundary-Layer Flow Turbulence Modeling

**5. FUNDING NUMBERS**

WU–505–62–52

**6. AUTHOR(S)**

Chi-Rong Wang

**7. PERFORMING ORGANIZATION NAME(S) AND ADDRESS(ES)**

National Aeronautics and Space Administration
Lewis Research Center
Cleveland, Ohio 44135–3191

**8. PERFORMING ORGANIZATION REPORT NUMBER**

E–7360

**9. SPONSORING/MONITORING AGENCY NAMES(S) AND ADDRESS(ES)**

National Aeronautics and Space Administration
Washington, D.C. 20546–0001

**10. SPONSORING/MONITORING AGENCY REPORT NUMBER**

NASA TM–105893

**11. SUPPLEMENTARY NOTES**

Prepared for the International Conference on Near-Wall Turbulence Flows, Tempe, Arizona, March 15–18, 1993.
Responsible person, Chi-Rong Wang, (216) 433–5865.

**12a. DISTRIBUTION/AVAILABILITY STATEMENT**

Unclassified - Unlimited
Subject Category 34

**12b. DISTRIBUTION CODE**

**13. ABSTRACT (Maximum 200 words)**

Baldwin-Lomax and $k$-$\varepsilon$ turbulence models were modified for use in Navier-Stokes numerical computations of Mach 2.9 supersonic turbulent-boundary-layer flows along compression ramps. The computational results of Reynolds shear stress profiles were compared with experimental data. The Baldwin-Lomax model was modified to account for the Reynolds shear stress amplification within the flow field. A hybrid $k$-$\varepsilon$ model with viscous sublayer turbulence treatment was constructed to predict the Reynolds shear stress profiles within the entire flow field. These modified turbulence models were effective for the computations of the surface pressure and the skin friction factor variations along an 8° ramp surface. The hybrid $k$-$\varepsilon$ model could improve the predictions of the Reynolds shear stress profile and the skin friction factor near the corner of a 16° ramp.

**14. SUBJECT TERMS**

Turbulence; Supersonic flow; Heat transfer

**15. NUMBER OF PAGES**

12

**16. PRICE CODE**

A03

| 17. SECURITY CLASSIFICATION OF REPORT | 18. SECURITY CLASSIFICATION OF THIS PAGE | 19. SECURITY CLASSIFICATION OF ABSTRACT | 20. LIMITATION OF ABSTRACT |
|---|---|---|---|
| Unclassified | Unclassified | Unclassified | |